Journal of Materials Chemistry A

ROYAL SOCIETY OF CHEMISTRY

PAPER

View Article Online
View Journal | View Issue

Cite this: J. Mater. Chem. A, 2022, 10, 20090

Porous polyaminoamides *via* an exotemplate synthesis approach for ultrahigh multimedia iodine adsorption†

Mohd. Avais and Subrata Chattopadhyay *

Received 4th April 2022
Accepted 29th July 2022

DOI: 10.1039/d2ta02708a

rsc.li/materials-a

Due to its long half-life and volatile nature, efficient removal of iodine from different media (such as vapor, organic solvents and water) is of primary importance for the sustainable production of nuclear energy. Herein we report our work on the preparation of porous polyaminoamides and their applications in the context of removal of iodine from different media. A series of porous polyaminoamides were prepared using sodium bicarbonate ($NaHCO_3$) as the exotemplate, where porosity of the resultant materials can be tuned by varying the amount of exotemplates. The materials show excellent thermal, chemical and radiation stability and iodine adsorption capacities in different media. The iodine adsorption capacity of the best material is determined to be 10.2 g g^{-1} in the vapor phase, 4.7 g g^{-1} in the organic phase and 5.9 g g^{-1} in aqueous medium. These are the benchmark values reported to date among all porous materials. Further their applicability in real world sea water matrices is also tested and the adsorption capacity is reported as 5.8 g g^{-1} and 5.6 g g^{-1} in basic and complex sea water matrices respectively. Excellent iodine adsorption capacity in addition to their thermal, chemical, and radiation stability makes them one of the best materials of choice for efficient iodine removal.

Introduction

To cope with the impending global energy demand, nuclear energy has emerged as one of the key sustainable and efficient alternatives to the existing greenhouse gas emitting technologies.[1] However, appropriate disposal of nuclear waste is a challenging issue in the context of the production of nuclear energy.[2,3] One of the major and important components in nuclear waste is iodine, which includes ^{129}I and ^{131}I. ^{129}I has a very long half-life (1.6×10^7 years) and thereby is of serious concern as the volatile iodine (both isotopes) can pollute the environment *via* both air and water, thereby causing serious concern to human health by affecting the metabolism.[4–7] Typically, in the vapor phase iodine exists as mainly molecular iodine (I_2) and a minor fraction remains as triiodide anions.[8] In contrary, polyiodide exists as major species in the aqueous phase, where triiodide is the major component.[9]

The conventional method to capture radioactive iodine involves the use of silver (Ag) based adsorbents.[10,11] The main drawback of the expensive Ag-based adsorbents is its lower efficiency.[12] The Ag–I bonds are less stable (bond energy ~ 66 kJ mol^{-1}), which leads to partial rerelease of iodine at 80 °C, which is a typical temperature for nuclear fuel reprocessing.[13] Further incorporation of expensive silver makes the overall process less cost-effective. This inspired researchers worldwide to explore new materials which are capable of capturing radioactive iodine efficiently from the off-gas mixtures. In the last decade, different porous materials such as covalent organic frameworks (COF),[14,15] metal organic frameworks (MOF),[16–18] and porous polymers (PP) appeared as some of the most promising materials showing excellent iodine capture efficiency.[19–23] Importantly it was noted that besides surface area (which always facilitates adsorption), functionality in the material backbone plays a more crucial role in the iodine adsorption ability,[23,24] as such adsorption generally occurs through physisorption processes *via* the local formation of charge transfer type interactions.[25,26] In this context, it was observed that functional amines when embedded within a polarizable network such as polyaromatic amines and polyaminoamides show excellent iodine adsorption ability.[27–30] However, most of the reported materials demonstrate iodine adsorption ability only in the vapor phase and organic solvents.[31–37] Materials which show significant iodine adsorption ability in water, are much less reported.[14,38,39] Rarely a material is reported that demonstrated iodine adsorption in all different media which include vapor phase, organic phase and aqueous phase.[40] Besides that in most cases, the iodine adsorption ability in the organic phase and water is lower and demands improvement.

Herein we report the design of porous hydrophobic polyaminoamides *via* an exotemplate synthesis approach.

Department of Chemistry, Indian Institute of Technology Patna, Bihta, Patna, 801106, Bihar, India. E-mail: sch@iitp.ac.in

† Electronic supplementary information (ESI) available. See https://doi.org/10.1039/d2ta02708a

Traditional use of sodium bicarbonate ($NaHCO_3$) as a foaming/blowing agent is well known to generate porosity in the materials and thereby enhance surface area.[41–44] However, excess blowing mostly leads to macropores. So here we used partial blowing by heating it at 100 °C.[45] 1,2-Diaminooctane was chosen as a hydrophobic monomer to synthesize the hydrophobic polyaminoamide network. We hypothesized that the hydrophobic surface will make the material hydrolytically stable, while the porous surface containing basic amine functionality in combination with polarizable amides will enable excellent iodine adsorption in different media. The porosity and surface area of the materials were tuned by the use of varying amounts of exotemplate. The prepared materials show excellent thermal, chemical, and radiation stability. The applications of these materials are thereafter studied to understand their ability to capture iodine in the vapor phase (resembling the fuel reprocessing conditions), organic phase and aqueous phase, which also include challenging matrices such as seawater.

Results and discussion

Preparation of porous polyamino-amides *via* an exotemplate synthesis approach

In the present work, porous polymers were synthesized using $NaHCO_3$ as an exotemplate (Scheme 1). To tune the porosity and achieve a better surface area, several materials were prepared by varying the content of exotemplate, such as 10 wt%, 20 wt%, 25 wt%, 30 wt%, and 40 wt%. Hydrophobic hyperbranched polyaminoamides (HBP) were generated initially *via* the reaction between diamino octane and bis-acrylamide (Fig. S1, S2 and Table S3†), which were later cross-linked in the presence of $NaHCO_3$ (as the exotemplate), while the exotemplate was embedded within the crosslinked matrix. Later, the freeze dried crosslinked material was heated at 100 °C for partial decomposition of $NaHCO_3$, with the release of CO_2, which gives a partial blowing effect. In the final step, the remaining $NaHCO_3$ (unreacted template) & Na_2CO_3 (side product) were removed by washing the cross linked material with water to prepare the final porous polymer. The removal of the sodium salt templates from the materials was confirmed *via* the EDX analysis, *via* monitoring the sodium content before and after washing (Fig. S3†). Using this approach, five different analogues (PP-1, PP-2, PP-3, PP-4, and PP-5) were prepared with the same composition but different porosity and surface area.

The synthesized porous polymers were characterized *via* solid state ^{13}C NMR and FTIR analyses (Fig. 1). ^{13}C NMR analysis (Fig. 1a) revealed the absence of any acrylamide peaks around 130 ppm and presence of peaks between 20 and 60 ppm (which are ascribed to octyl chains and methylene $-CH_2-$ moieties)-supporting the formation of polyamino-amide networks *via* aza-Michael reactions. Additionally, FTIR analysis (Fig. 1b) confirms the molecular details, such as peaks around 3300 cm^{-1} (N–H stretching) and 1650 cm^{-1} (C=O stretching) are characteristic of the amide bond, peaks around 2920 cm^{-1} are characteristic of methylene C–H stretching vibration and peaks around 1130 cm^{-1} are characteristic of the newly formed C–N bonds *via* aza-Michael addition. Furthermore, representative XPS analysis (Fig. 1c) reveals the presence of C 1s, N 1s, and O 1s peaks around ~285.0 eV, ~399.0 eV and ~531.0 eV respectively. These results unambiguously confirm the molecular structure of the PPs.

The porosity and surface area of the porous network were studied using low temperature nitrogen adsorption desorption isotherm (BET analysis) and mercury intrusion porosimetry (MIP) (Fig. 2). While BET is useful to analyze the overall surface area and micropore (from 0.5–2 nm) and smaller mesopore content, MIP is more useful to analyze the larger mesopores and macroporous content and is useful to quantify the overall porosity. Besides the porosity and surface area analysis, the aim of the study was also to investigate the effect of the exotemplate content on the formation of a material with optimum surface area. As shown in Fig. 2c, d and e, the surface area and total pore volume (both by NLDFT and BJH analyses) increase with the increase of the $NaHCO_3$ content till 25 wt% (PP-3) and pore volume further decreases if the $NaHCO_3$ content increases beyond 25 wt%. MIP analysis (Fig. 2a and b) in the context of

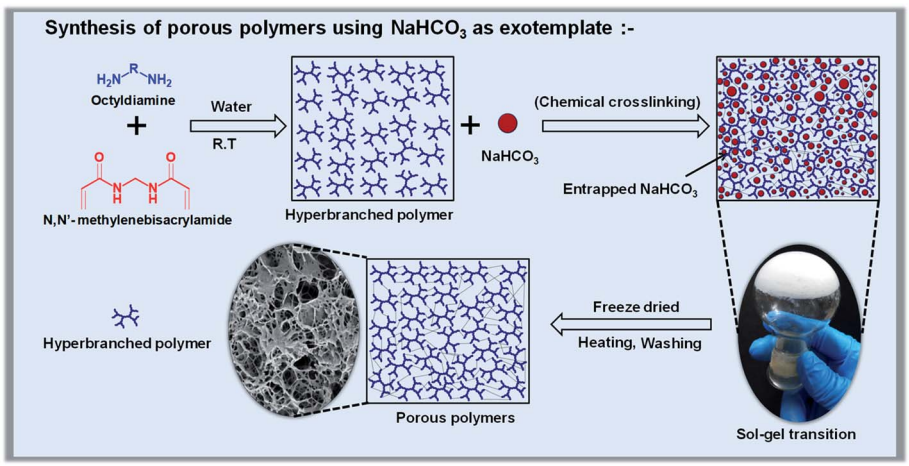

Scheme 1 Synthesis of porous polyaminoamides using $NaHCO_3$ as the exotemplate.

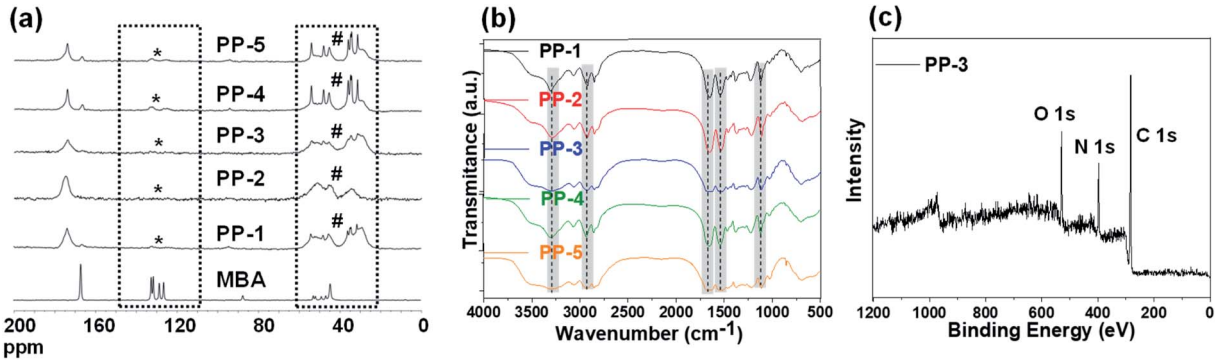

Fig. 1 Molecular characterization of porous polymers *via* (a) solid state ^{13}C NMR spectra, (b) IR spectra and (c) XPS spectra.

pore volume and porosity analysis also supported the same trend. Further, NLDFT and BJH analyses reveal that the materials are predominantly mesoporous with a very little micropore content (Table S4†). Through all the analyses, it can be ambiguously concluded that PP-3 emerged as the best polyaminoamide with a surface area of 146 m^2 g^{-1} and overall porosity of 94% (Fig. 2f). The details of the analysis for all materials are tabulated in Table S4.†

Further the porous morphology of the polymers was visualized by FESEM analysis (Fig. S4†). The SEM micrographs also supported better pore formation for PPR-3. Furthermore, the micrographs also revealed open pore porous morphology (inset, Fig. 3a). HRTEM analysis (Fig. 3b) revealed the presence of very small micropores, and the size of the micropores is mostly around 0.3 nm or less, which explains why such pores are not detectable *via* nitrogen adsorption desorption analysis.[46]

Thermal stability of the porous polymers was affirmed *via* thermogravimetric analysis (TGA), confirming the excellent thermal stability of the materials till 260 °C (Fig. S5†). Further, their chemical inertness in different solvents was analyzed *via* gravimetric methods, followed by further characterization of the post treated materials using FESEM and IR analyses. Gravimetric analysis confirms that there is no significant loss of the materials when exposed to various solvents, such as THF, chloroform, DMSO, methanol, DMF and aqueous medium (all types including acidic, basic and neutral aqueous mediums were used) (Fig. S6†). IR (Fig. S7†) and FESEM (Fig. S8†) analysis of the post-treated materials affirms that the molecular structure and morphology of the materials remain intact. The excellent chemical and thermal stability of the materials ensures that the materials can be useful for practical applications.

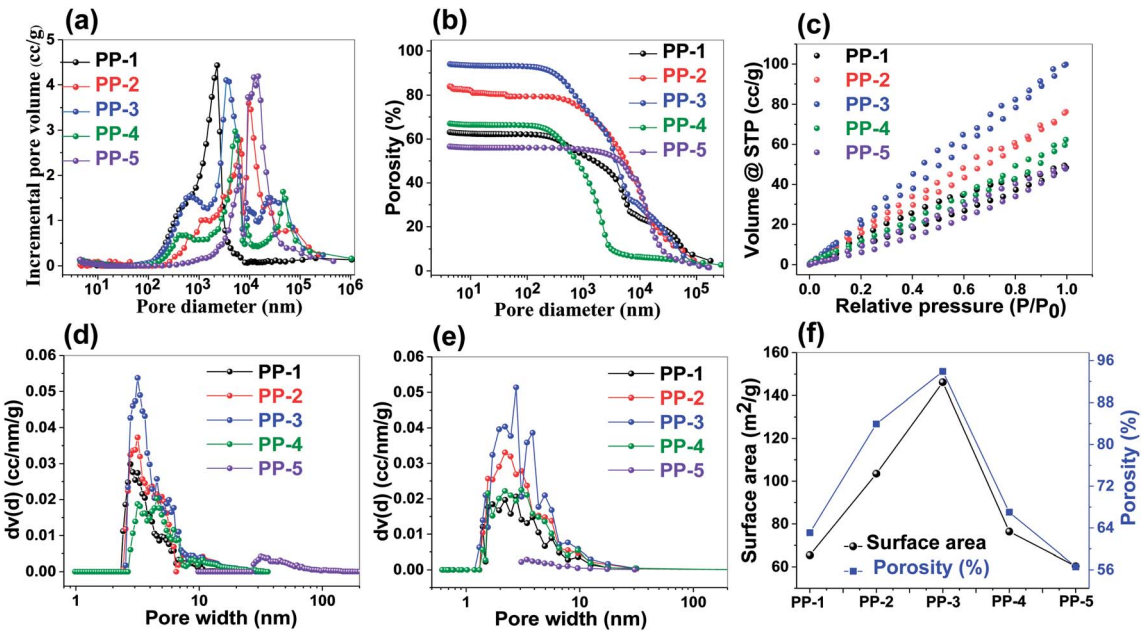

Fig. 2 Porosity and surface area analysis of the porous polymers (a) pore size distribution by mercury porosimetry, (b) calculated overall porosity, (c) nitrogen adsorption desorption isotherms at 77 K, pore size distribution of the PP as determined by (d) DFT and (e) the BJH method and (f) comparison graph between the porosity and surface area of all porous polymers.

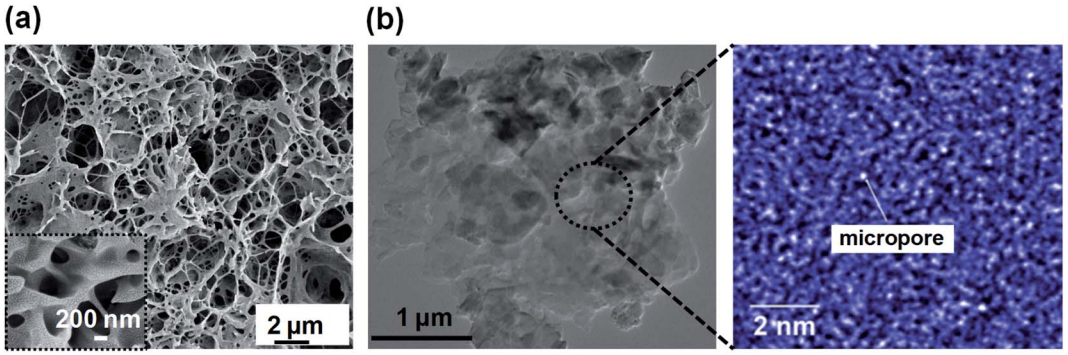

Fig. 3 (a) FESEM and (b) HRTEM micrographs of PP-3.

Iodine adsorption in the vapor phase. To investigate the volatile iodine capture capacity of PPs, the gravimetric method was used for analysis. Porous polymers were exposed to iodine vapor at 80 °C under ambient pressure. This was a typical lab setup, nearly resembling actual nuclear-fuel reprocessing. Gravimetric measurements were performed at regular time intervals, and the results showed that almost 80% iodine was adsorbed in the vapor phase within first 20 h. After approximately 72 h adsorption equilibrium was reached (Fig. 4a). The iodine adsorption capacity was determined to be 7.9, 9.5, 10.2, 9.2 and 6.2 g g^{-1} for PP-1, PP-2, PP-3, PP-4 and PP-5, respectively. PP-3 exhibited the highest iodine uptake value of 10.2 g g^{-1} among the different prepared polymers mainly due to their higher surface area & porosity among all five analogues. Remarkably, this experimentally calculated adsorption capacity is among the benchmark values reported in the literature for all kinds of porous materials (Table S5 and Fig. S9†). Moreover, the kinetics of iodine adsorption was investigated *via* data fitting using pseudo-first-order and pseudo-second-order kinetic models (Fig. S10†). Excellent correlation coefficient (R^2) and rate constant (k_2) values were determined using the pseudo-second-order kinetic model. More details of different parameters are reported in Table S6.† The iodine loaded polymer (PP-3-I_2) was investigated using FESEM and EDX analysis (Fig. 4c). FESEM micrographs indicated iodine adsorbed porous surface morphology and the presence of the iodine element was confirmed by EDX analysis. The TGA of the PP3–I_2 polymer was performed and the thermogram was compared with the thermogram of the respective porous polymer (Fig. 4b and S11†). Notably, TGA of the iodine loaded porous polymer exhibited a drastic weight loss below 260 °C, which is absent in the actual porous polymer and can be ascribed to the weight loss due to release of iodine. The calculated iodine weight losses are 4.5, 8.4, 9.5, 8.1 and 4.4 g g^{-1} for the PP-1, PP-2, PP-3, PP-4, and PP-5, respectively, which are comparable to the adsorption of iodine in the vapor phase by the gravimetric method mentioned above.

To further understand the utility of the porous polymer adsorbents in real-time applications, we looked into PP-3's adsorption selectivity for iodine vapor against water vapor and organic solvent vapor. To test this for the PP-3 polymer, the adsorption of iodine from a binary combination of vapors (at atmospheric pressure, a mixture of iodine and other competing vapors such as water, ethanol, hexane, and tetrahydrofuran) was examined. As shown in Fig. S12,† the presence of various water and organic vapors has a negligible effect on the adsorption of iodine vapor. The uptake performance for iodine vapor was found to be retained by 76, 72, 76, and 74% in the presence of water, ethanol, hexane, and tetrahydrofuran vapors, respectively. The results showed that the PPs have excellent utilization potential for the removal of iodine in challenging gas mixtures.

Iodine removal from the organic phase. The iodine adsorption capacity of PPs was further probed in aprotic solvent (*n*-hexane). Adsorption isotherms (Fig. 5a) clearly revealed higher iodine adsorption capacity of PP-3 when compared with other porous polymers (PP-1, PP-2, PP-4, and PP-5) as expected. It was

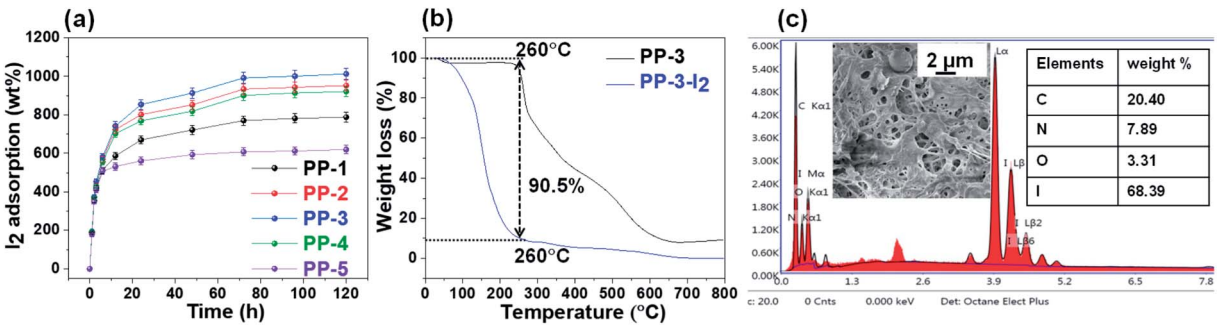

Fig. 4 (a) Iodine adsorption of PPs in the vapor phase, (b) TGA analysis and (c) SEM and EDX analyses of iodine adsorbed porous polymers.

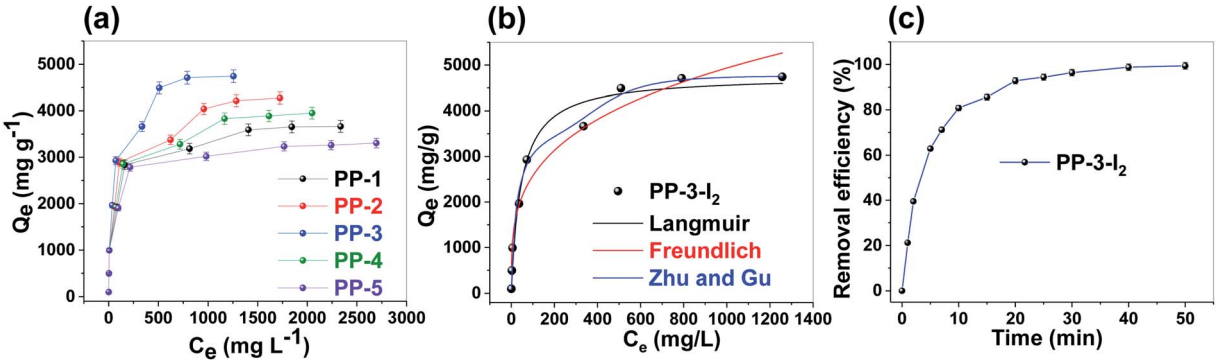

Fig. 5 Iodine adsorption study in *n*-hexane: (a) adsorption isotherms of different porous polymers, (b) Langmuir, Freundlich and Zhu and Gu adsorption isotherm models for PP-3, and (c) iodine adsorption kinetics.

noticed that iodine adsorption capacity for all PPs increased quickly at the initial stage and equilibrium was established within 24 h. The highest adsorption capacity of PP-3 for I_2 was calculated to be 4.7 g g^{-1} (experimentally). This emerged as one of the best reported porous materials in the context of iodine adsorption in organic solution when compared with the recent literature (Table S7 and Fig. S13†). To study further details, the iodine adsorption isotherms were fitted using Langmuir and Freundlich isotherm models (Fig. 5b and S14†). The details of different parameters are summarized in Table S8.† The results indicate that the iodine adsorption isotherm fitted well with the Langmuir model when compared to the Freundlich model with better R^2 values (0.94–0.97). Moreover, the calculated adsorption capacity values for all the PPs from the Langmuir isotherm model were closer to the experimentally obtained values. In addition, very high iodine adsorption capacity of the polyaminoamide porous polymers despite their moderate surface area is difficult to explain from the Langmuir isotherm only. To study further, the adsorption isotherm is fitted with the Zhu-Gu adsorption isotherm model (Fig. 5b and S14†). The calculated parameters are reported in Table S9.† The calculated R^2 value is 0.99 which is better compared to the Langmuir model. The calculated maximum adsorption capacity (4766 mg g^{-1}) also closely matches the experimentally obtained maximum adsorption capacity (4742 mg g^{-1}). This indicated polyiodide cluster formation during the adsorption process.

In the next stage, kinetics of iodine adsorption in *n*-hexane was studied using UV-Vis spectroscopy (Fig. S15a†). The data clearly revealed fast iodine removal from organic media ~80% iodine was removed within 10 minutes, while more than 95% iodine was removed within 30 minutes (Fig. 5c). Moreover, the removal kinetics followed a pseudo-second-order model with a better correlation coefficient (R^2) value of 0.99 compared to the pseudo-first-order kinetic model (Fig. S15b, c and Table S10†).

Iodine adsorption in aqueous solution. Due to an increase in industrial development, huge quantities of waste, a part of radioactive iodine waste is discharged into the sea, which threatens aquatic life and the ecosystem.[4] Hence, removal of iodine from water is essential for the safety of aquatic life and surroundings. Limited reports are published that discuss the adsorption of iodine in aqueous medium. The good chemical stability of PPs in various aprotic to protic solvents, including water and excellent adsorption capacity in vapour and organic phases inspired us to analyze their adsorption performance in aqueous solution. For this, 2.5 mg of PPs were immersed in I^{3-} aqueous solution (which is prepared *via* mixing of equal proportions of KI and iodine in water) with constant stirring at 500 rpm for 24 h. After equilibrium is reached, the concentration of the solution measured by UV-Vis spectroscopy and adsorption capacity was calculated (calculated using eqn S4 and S5, ESI†). The corresponding calculated adsorption capacity was found to be 4.2, 5.8, 5.9, 5.1 and 4 g g^{-1} for PP-1, PP-2, PP-3, PP-4 and PP-5, respectively (Fig. 6a). Furthermore, these high uptake values were studied using various adsorption isotherm models such as the Langmuir, Freundlich, and Zhu-Gu models (Fig. 6b and S16†). The theoretical adsorption capacity using various isotherm models matches well with calculated experimental values. Better R^2 values (0.97–0.99) were found with the Zhu-Gu model for all the porous polymers with the k_3 value higher than one, which indicated the formation of polyiodide clusters (Tables S11 and S12†). All these I_3^- adsorption capacity values were further reconfirmed by the titration method and similar results were observed, *i.e.* 4.2, 5.7, 5.8, 5 and 3.9 g g^{-1} for PP-1, PP-2, PP-3, PP-4 and PP-5, respectively. It is important to note that these are the best among all reported porous materials considering the noted adsorbents in aqueous solution (Table S13 and Fig. S17†). Similar to the earlier trend, PP-3 emerged as the best material among the five prototypes and to the best of our knowledge this is possibly the best material reported to date considering it's iodine capture efficiency in all three different media. In the next stage, kinetics of I_3^- adsorption in water was analyzed using UV-Vis spectroscopy (Fig. S18a†). The obtained removal efficiency clearly indicates ultrafast iodine removal from water media ~90% iodine was removed within 5 minutes, while more than 98% iodine was removed within 10 minutes (Fig. 6c). Moreover, the removal kinetics followed a pseudo-second-order model with a better correlation coefficient value of 0.99 over the pseudo-first-order kinetic model (Fig. S18b, c and Table S14†).

To highlight the excellent performance of PP polymers in removing iodine anions, the effects of various adsorption parameters, including pH and other competitive anions, were

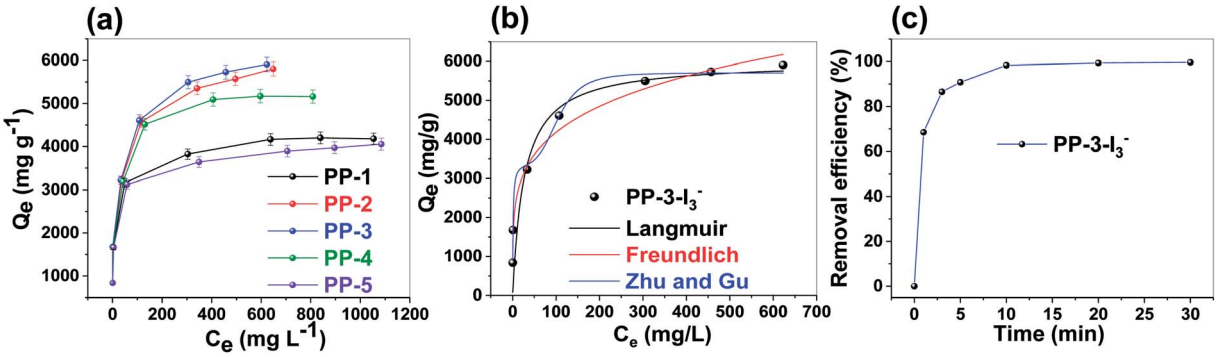

Fig. 6 Iodine adsorption study in water: (a) adsorption isotherms of different porous polymers, (b) Langmuir, Freundlich and Zhu and Gu adsorption isotherm models for PP-3, and (c) iodine adsorption kinetics.

studied to investigate the adsorption capacity of the PP polymers. The effects of pH values (ranging from 4 to 9.2) on iodine removal in water were studied using a 500 ppm initial iodine concentration. As shown in Fig. S19,† removal efficiencies remained nearly constant within the pH range of 4–7.4; the influence of pH on removal efficiency was negligible, demonstrating that mild acid conditions have no discernible impact on the adsorption of iodine. However, the removal efficiency showed a slight decrease (~5%) with increasing pH in alkaline environments.[47]

Further, we investigated the selectivity of PP-3 for I_3^- adsorption to gain a sense of usefulness of the porous polymer adsorbents in real-time applications. Contaminated wastewater contains various counter anions, such as nitrate (NO_3^-), chloride (Cl^-), acetate (CH_3COO^-), bromide (Br^-), sulphate (SO_4^{2-}), and fluoride (F^-), which can obstruct the adsorption of I_3^-. To test this for the current polymer, the adsorption of I_3^- from a binary combination of anions (equimolar solution of I_3^- and other competing ions such as NO_3^-, Cl^-, CH_3COO^-, Br^-, SO_4^{2-}, and F^-) was examined. The results demonstrated that the presence of various anions has a negligible effect on the adsorption of I_3^- (Fig. 7a). The removal performance for I_3^- was found to be retained by >95% for the PP-3 porous polymer in all the experiments.

Additionally, we also estimated the binding affinity constant value (K_d) for all binary-competing mixtures, which was found to be in the order of ~10^4 mL g^{-1} (Fig. 7b). This result shows that PP-3 porous polymers have exceptionally high binding affinity for I_3^- in the presence of other competing anions.[48,49] We also probed how well the polymer removed I_3^- in the presence of several anions (NO_3^-, Cl^-, CH_3COO^-, Br^-, SO_4^{2-}, and F^-) at the same time (more details given in the Experimental section). Further, when compared to binary-mixture-based selectivity experiments, PP-3 revealed similar absorption capacity and performance retention.

Further, the adsorption of iodine from a real-world matrix (sea water) was examined using the PP-3 polymer. First, basic and complex seawater samples were prepared in the laboratory using varying salt proportions (details in the Experimental section). The PP-3 polymer was immersed in this solution (which was laced with iodine), and after 24 h, the supernatant was centrifuged and the concentration was analyzed using UV-Vis spectroscopy. Furthermore, the polymer has an absorption capacity of 5.8 and 5.6 g g^{-1} for I_3^- anions from basic and complex solutions, which is remarkable given the difficult matrix of seawater (Fig. 7c).

Besides that, considering the matrix's high quantities of competing ions and fouling agents, the K_d was determined to be in the order of ~10^4 mL g^{-1}, which is extraordinarily high (Fig. 7c) and supports very well its iodine adsorption ability. Overall, the results demonstrate that the PP porous polymers can be used in real-world samples.

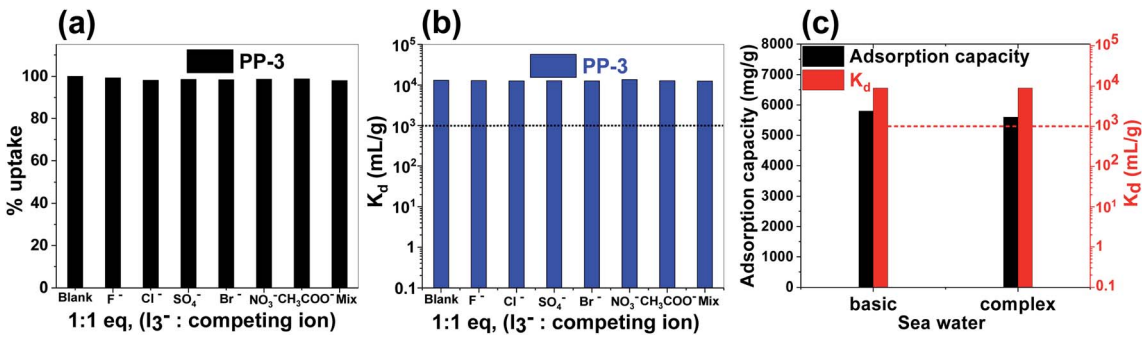

Fig. 7 (a) Uptake percent for I_3^- anions in the presence of other competing anions, (b) distribution coefficient (K_d) graph and (c) I_3^- adsorption capacity from the basic and complex seawater and the corresponding distribution coefficient value (K_d).

Mechanism of iodine adsorption

The ultra-high iodine adsorption by the PP polymer could be elucidated by the formation of a polyiodide charge transfer complex between iodine and polymer backbone functionalities. The presence of nitrogen and oxygen atoms in the network, which interacts with I_2 molecules, results in the formation of a polyiodide ion complex *via* charge transfer between the non-bonding orbitals of nitrogen atoms in the polymer backbone and the anti-bonding molecular orbital of iodine (Fig. S20†). This outer charge complex transforms into an inner charge complex and is responsible for more iodine to produce the polyiodide charge ion complex,[20,50] which has been investigated by ESR, XPS and Raman spectra analyses. ESR analysis reveals the presence of strong paramagnetic signals in the iodine adsorbed polymer sample which were actually absent in the porous polymer before adsorption (Fig. S21†). The paramagnetic signals of the iodine species in the charge–transfer complexes are typically not observed at room temperature because of the high anisotropy and quick electron-spin relaxation.[51] As a result, the appearance of the paramagnetic signals after iodine adsorption supports charge transfer interactions between PP-3 and iodine.[52] Next, XPS and Raman spectroscopy were used to exhibit the nature of the chemical binding between polymer networks and iodine molecules. Fig. 8a depicts the full survey XPS spectra of PP-3 before and after iodine adsorption. The iodine adsorbed PP-3-I_2 exhibited additional peaks around at ~618 and ~630 eV which were attributed to the chemical bonding between the polymer backbone and iodine. These peaks are further elucidated in the high resolution I3d and I5d spectra (Fig. 8c). There are two types of peaks: the I_2 species at 619.8 and 629.6 eV, while the peaks found at 618.2 and 631.4 eV are attributed to the polyiodide anion.[22,53]

These results reveal the coexistence of I_2, I_3^- and I_5^- and insertion of these iodine orbital peaks confirmed the adsorption of iodine on the network surfaces. In addition, C 1s spectra of PP-3-I_2 (Fig. S22a†), C–C, C–N, and C=O peaks appeared at 284.5, 285.9 and 287.8 eV, which is a slight shift compared to PP-3 (before the iodine adsorbed polymer). However, a peak at 531.3 eV (Fig. S22b†), corresponding to O 1s, appeared in the spectrum of PP-3-I_2, which is shifted slightly compared to PP-3. Importantly, N 1s spectra (Fig. 8b) also indicated that the adsorption of iodine on the PP-3 polymer led to 0.6 eV shift from 399.0 to 399.6 eV at the N 1s core level,[54] showing that amines present on the porous polymer surface interacted with iodine molecules. The formation of a new peak at 401.5 eV which was related to the N–I bond supported the establishment of polyiodide charge–transfer complexes between amine N and iodine molecules.[55] Moreover, the formation of the polyiodide charge transfer complex can be further confirmed by Raman spectroscopy (Fig. 8d). The characteristic peaks at ~108 and ~148 cm^{-1} were ascribed to the stretching vibrations of I_3^- and I_5^-, respectively.

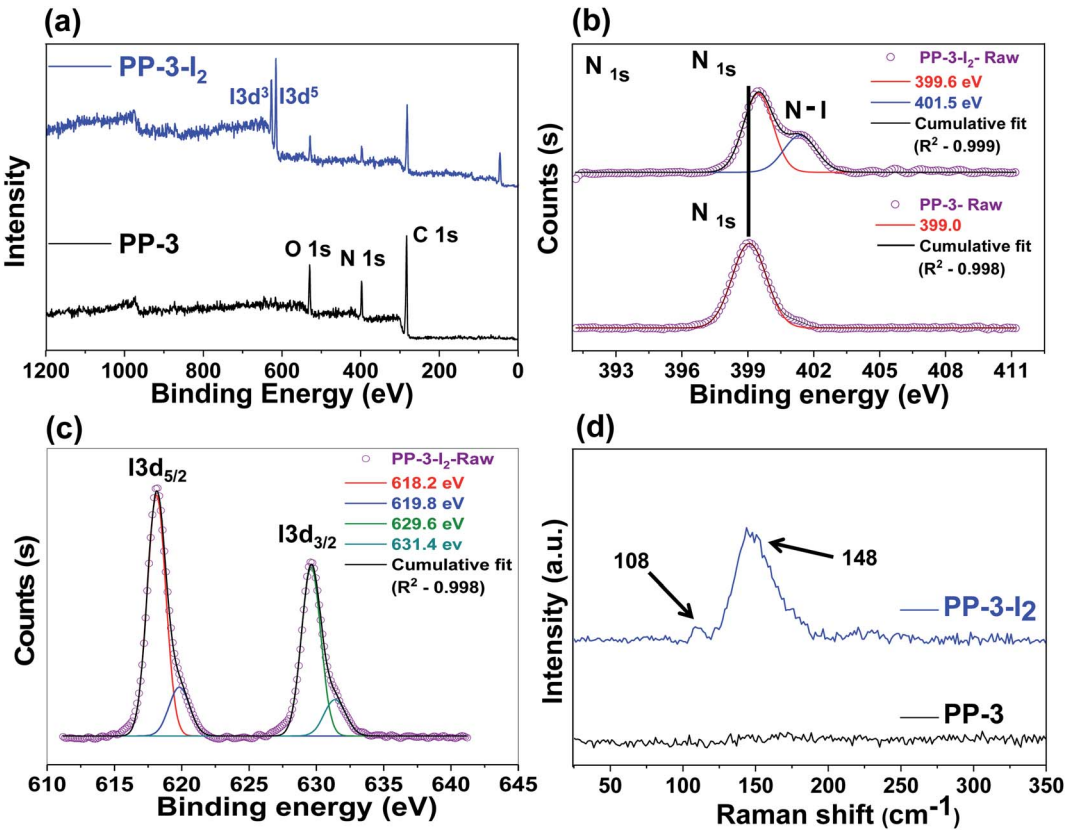

Fig. 8 XPS survey spectra of PP-3 and PP-3-I_2 (a) full spectra, (b) N 1s, (c) I 3d, and (d) Raman spectra analysis.

Reusability

Reversibility of iodine adsorption by porous materials is essential for their effective reuse in the context of sustainable and cost-effective practical application. To study this the iodine loaded porous polymers were first treated to release the adsorbed iodine completely and thereafter, reused for consecutive adsorption. For the current materials, iodine desorption was executed in two different ways—(i) simple heating at 140 °C and (ii) treating the iodine adsorbed materials in methanol. In the first method, the iodine desorption study was performed by first heating the iodine-loaded PP-3-I_2 polymer at 140 °C under ambient pressure for 2 days. The corresponding iodine release percentage was determined by calculating the weight changes in the PP-3-I_2 polymer (Fig. 9a). The release kinetics study clearly revealed that within 30 minutes, ~60% of the iodine was desorbed and approximately 95% of the iodine was released within the next 24 h.

In the second process, iodine release in a methanolic solution of tetrabutylammonium bromide under ambient conditions was investigated using UV-Vis spectroscopy (Fig. 9b). Due to the continuous release of iodine trapped in the PP-3-I_2 polymer, the color of the solution gradually changed from white to light yellow and finally dark yellow over time. The UV-visible spectra of the supernatants revealed two absorbance maxima at 287 and 352 nm, indicating the presence of polyiodide anions. As exhibited in Fig. 9b, a gradual increase in the intensity of both peaks (which at 287 and 352 nm) with time was noted, up to 360 minutes.

There was no discernible increase in the intensity of these peaks after 360 minutes, indicating that equilibrium conditions had been established. To affirm the complete release of the iodine in solution from the porous polymer FESEM and EDX analyses were performed. FESEM study revealed that the porous surface morphology was retained and EDX analysis demonstrated the removal of the iodine element from the porous polymer matrix post-treatment (Fig. 9c).

After desorption in solution, the recovered PP-3-I_2 was consequently used for the next cycle of iodine adsorption. The results demonstrated that after the first cycle, the relative adsorption capacity was 93%, and after three cycles, more than 90% efficiency was retained (Fig. 9d). This indicates that the polymer can be effectively reused for at least three consecutive cycles.

Irradiation stability

To validate the practical applicability of the adsorbents, their radiation stability against γ-irradiation was studied. Additionally, their stability against UV, sunlight (weathering), and X-ray (considering the fact that both X-ray and radioactive iodine are used in cancer treatment) was investigated. The polymer's stability was analyzed by solid-state ^{13}C-NMR, FTIR, and FESEM to confirm the retention of their molecular structure and morphology after treatment. Thereafter, iodine adsorption was also performed, to confirm their performance. The solid-state ^{13}C-NMR (Fig. S23†), IR (Fig. S24†), and FESEM (Fig. S25†) analyses of the post-treated materials affirm that the molecular

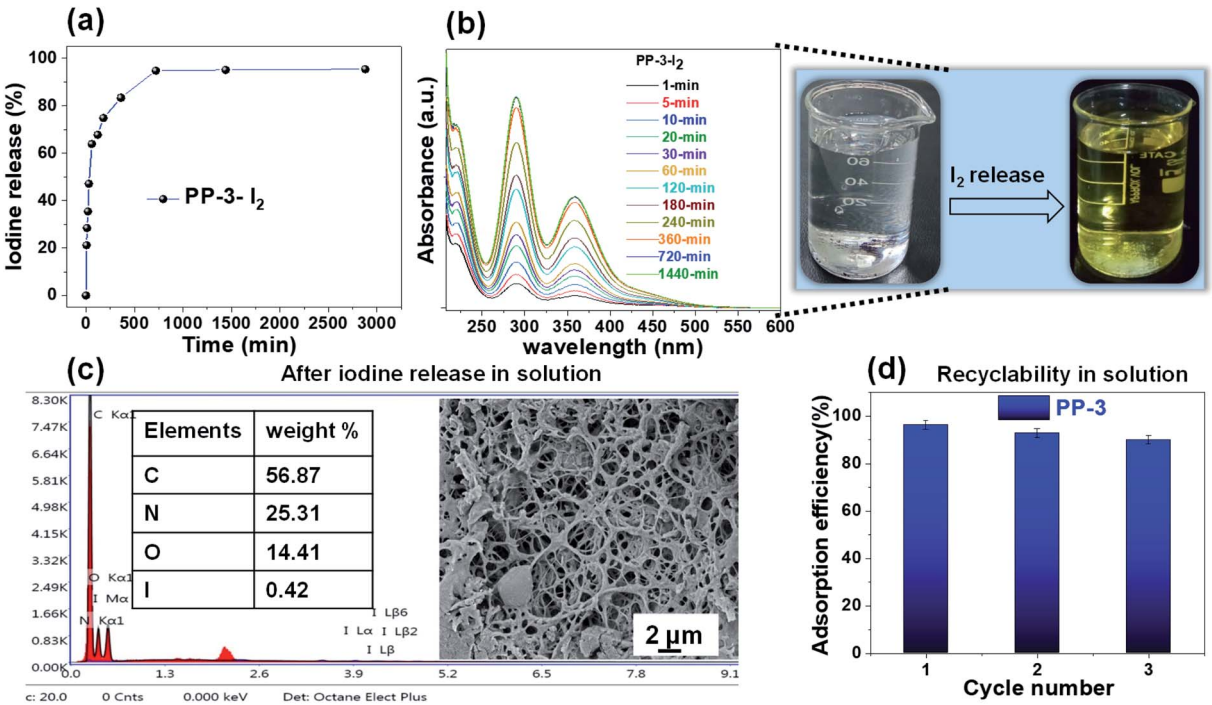

Fig. 9 (a) Iodine release kinetics with heating at 140 °C, (b) UV spectra of rapid iodine release from PP-3-I_2 in methanol (image showing the visual color change for iodine release), and (c and d) EDX analysis of PP-3 after iodine release (FESEM image inset) and reusability of PP-3 for iodine adsorption, respectively in solution.

structure and surface morphology of the materials remain intact. To ascertain the irradiation stability of PP-3, the iodine adsorption performance in multimedia phases both before and after irradiation was examined (Fig. S26†). Interestingly, PP-3 preserved 98, 91, 93, and 90% of the original adsorption capacity in the vapor phase and 99, 96, 98, and 93% in aqueous media and 97, 92, 95, and 91% in the organic phase after sunlight, UV, X-ray, and γ-irradiation, respectively. The results demonstrated that the synthesized porous polyaminoamide polymer could be effectively used in challenging radiation environments.[52]

Conclusion

In summary, we have investigated in detail the synthesis of porous polyaminoamides using $NaHCO_3$ as the exotemplate. Porosity and surface area of the polymers can be tuned *via* varying the exotemplate content during synthesis. The hydrophobic polyaminoamides show exceptional chemical stability in various protic & aprotic solvents and thermal stability was noted till 260 °C. The polymers exhibit excellent iodine adsorption capacity in all different media which includes vapor phase, organic phase and water. The highest adsorption capacities in the current work are noted as 10.2 g g^{-1} in the vapor phase, 4.7 g g^{-1} in organic solution (*n*-hexane) and 5.9 g g^{-1} in aqueous media, which are among the highest reported values to date to the best of our knowledge. Moreover, the polymer exhibited ultra-fast adsorption in water; ∼99% of triiodide ions were adsorbed within 10 minutes. Additionally, it showed unprecedented selective adsorption of triiodide ions in the presence of huge excesses of other anions such as F^-, NO_3^- and SO_4^{2-} *etc.* The calculated distribution coefficient (k_d, 8.9 × 10^3 mL g^{-1}) value revealed the good affinity towards iodine adsorption from seawater-spiked solutions. Finally, porous polymers exhibited good recyclability and radiation stability, which makes them practically useful and cost-effective.

Author contributions

All experiments and analyses were performed by Mohd. Avais. Subrata Chattopadhyay conceptualized and supervised the work. The manuscript was written through contributions of all authors. All authors have given approval to the final version of the manuscript.

Conflicts of interest

The authors declare no competing financial interest.

Acknowledgements

The authors thank Indian Institute of Technology Patna (IITP) for generous financial and infrastructural support. Md. Avais thanks IITP for a research Fellowship. S.C. also acknowledges CSIR grant-in-aid, scheme no. 02(0370)/19/EMR-II, for financial support. The authors gratefully acknowledge SAIF, IITP for NMR analysis and Sprint Testing Solution, Bombay for the XPS analysis. The authors also thank Akshar gamma steriles LLP (Maharashtra) for gamma radiation and Dr Koteswaraarao Jadda (at IITP) and Mohtaram Danish (at AMU) for their help with mercury intrusion porosimetry and ESR experiments, respectively.

References

1 T. Findlay, *The Future of Nuclear Energy to 2030 and its Implications for Safety, Security and Nonproliferation*. 2010.
2 N. Yoshida and J. Kanda, Tracking the Fukushima radionuclides, *Science*, 2012, **336**(6085), 1115–1116.
3 B. J. Riley, J. D. Vienna, D. M. Strachan, J. S. McCloy and J. L. Jerden Jr, Materials and processes for the effective capture and immobilization of radioiodine: A review, *J. Nucl. Mater.*, 2016, **470**, 307–326.
4 F. C. Küpper, M. C. Feiters, B. Olofsson, T. Kaiho, S. Yanagida, M. B. Zimmermann, L. J. Carpenter, G. W. Luther III, Z. Lu and M. Jonsson, Commemorating two centuries of iodine research: an interdisciplinary overview of current research, *Angew. Chem., Int. Ed.*, 2011, **50**(49), 11598–11620.
5 W. Xie, D. Cui, S.-R. Zhang, Y.-H. Xu and D.-L. Jiang, Iodine capture in porous organic polymers and metal–organic frameworks materials, *Mater. Horiz.*, 2019, **6**(8), 1571–1595.
6 K. S. Subrahmanyam, D. Sarma, C. D. Malliakas, K. Polychronopoulou, B. J. Riley, D. A. Pierce, J. Chun and M. G. Kanatzidis, Chalcogenide aerogels as sorbents for radioactive iodine, *Chem. Mater.*, 2015, **27**(7), 2619–2626.
7 Y. Benamrane, J.-L. Wybo and P. Armand, Chernobyl and Fukushima nuclear accidents: what has changed in the use of atmospheric dispersion modeling?, *J. Environ. Radioact.*, 2013, **126**, 239–252.
8 A. Saiz-Lopez, J. M. Plane, A. R. Baker, L. J. Carpenter, R. von Glasow, J. C. Gómez Martín, G. McFiggans and R. W. Saunders, Atmospheric chemistry of iodine, *Chem. Rev.*, 2012, **112**(3), 1773–1804.
9 P. H. Svensson and L. Kloo, Synthesis, structure, and bonding in polyiodide and metal iodide−iodine systems, *Chem. Rev.*, 2003, **103**(5), 1649–1684.
10 K. W. Chapman, P. J. Chupas and T. M. Nenoff, Radioactive iodine capture in silver-containing mordenites through nanoscale silver iodide formation, *J. Am. Chem. Soc.*, 2010, **132**(26), 8897–8899.
11 R. M. Asmussen, J. Matyáš, N. P. Qafoku and A. A. Kruger, Silver-functionalized silica aerogels and their application in the removal of iodine from aqueous environments, *J. Hazard. Mater.*, 2019, **379**, 119364.
12 J. S. Hoskins, T. Karanfil and S. M. Serkiz, Removal and sequestration of iodide using silver-impregnated activated carbon, *Environ. Sci. Technol.*, 2002, **36**(4), 784–789.
13 J. Wang, Z. Li, Y. Wang, C. Wei, K. Ai and L. Lu, Hydrogen bond-mediated strong adsorbent–I3− interactions enable high-efficiency radioiodine capture, *Mater. Horiz.*, 2019, **6**(7), 1517–1525.
14 Y. Lin, X. Jiang, S. T. Kim, S. B. Alahakoon, X. Hou, Z. Zhang, C. M. Thompson, R. A. Smaldone and C. Ke, An elastic

hydrogen-bonded cross-linked organic framework for effective iodine capture in water, *J. Am. Chem. Soc.*, 2017, **139**(21), 7172–7175.

15 K. Jie, Y. Zhou, E. Li, Z. Li, R. Zhao and F. Huang, Reversible iodine capture by nonporous pillar [6] arene crystals, *J. Am. Chem. Soc.*, 2017, **139**(43), 15320–15323.

16 G. M. Espallargas and E. Coronado, Magnetic functionalities in MOFs: from the framework to the pore, *Chem. Soc. Rev.*, 2018, **47**(2), 533–557.

17 K. Shen, L. Zhang, X. Chen, L. Liu, D. Zhang, Y. Han, J. Chen, J. Long, R. Luque and Y. Li, Ordered macro-microporous metal-organic framework single crystals, *Science*, 2018, **359**(6372), 206–210.

18 Z. Ji, H. Wang, S. Canossa, S. Wuttke and O. M. Yaghi, Pore chemistry of metal–organic frameworks, *Adv. Funct. Mater.*, 2020, **30**(41), 2000238.

19 Y. H. Abdelmoaty, T.-D. Tessema, F. A. Choudhury, O. M. El-Kadri and H. M. El-Kaderi, Nitrogen-rich porous polymers for carbon dioxide and iodine sequestration for environmental remediation, *ACS Appl. Mater. Interfaces*, 2018, **10**(18), 16049–16058.

20 S. Xiong, X. Tang, C. Pan, L. Li, J. Tang and G. Yu, Carbazole-bearing porous organic polymers with a mulberry-like morphology for efficient iodine capture, *ACS Appl. Mater. Interfaces*, 2019, **11**(30), 27335–27342.

21 X.-H. Xu, Y.-X. Li, L. Zhou, N. Liu and Z.-Q. Wu, Precise fabrication of porous polymer frameworks using rigid polyisocyanides as building blocks: from structural regulation to efficient iodine capture, *Chem. Sci.*, 2022, **13**, 1111–1118.

22 Y. Zhu, Y.-J. Ji, D.-G. Wang, Y. Zhang, H. Tang, X.-R. Jia, M. Song, G. Yu and G.-C. Kuang, BODIPY-based conjugated porous polymers for highly efficient volatile iodine capture, *J. Mater. Chem. A*, 2017, **5**(14), 6622–6629.

23 T. Geng, C. Zhang, M. Liu, C. Hu and G. Chen, Preparation of biimidazole-based porous organic polymers for ultrahigh iodine capture and formation of liquid complexes with iodide/polyiodide ions, *J. Mater. Chem. A*, 2020, **8**(5), 2820–2826.

24 X. Qian, Z.-Q. Zhu, H.-X. Sun, F. Ren, P. Mu, W. Liang, L. Chen and A. Li, Capture and reversible storage of volatile iodine by novel conjugated microporous polymers containing thiophene units, *ACS Appl. Mater. Interfaces*, 2016, **8**(32), 21063–21069.

25 Y. Xu, S. Jin, H. Xu, A. Nagai and D. Jiang, Conjugated microporous polymers: design, synthesis and application, *Chem. Soc. Rev.*, 2013, **42**(20), 8012–8031.

26 Z. Yan, Y. Yuan, Y. Tian, D. Zhang and G. Zhu, Highly efficient enrichment of volatile iodine by charged porous aromatic frameworks with three sorption sites, *Angew. Chem.*, 2015, **127**(43), 12924–12928.

27 T. Geng, Z. Zhu, W. Zhang and Y. Wang, A nitrogen-rich fluorescent conjugated microporous polymer with triazine and triphenylamine units for high iodine capture and nitro aromatic compound detection, *J. Mater. Chem. A*, 2017, **5**(16), 7612–7617.

28 M. Avais, S. Kumari and S. Chattopadhyay, Degradable and processable polymer monoliths with open-pore porosity for selective CO_2 and iodine adsorption, *Soft Matter*, 2021, **17**(26), 6383–6393.

29 M. Avais and S. Chattopadhyay, Hierarchical Porous Polymers via a Microgel Intermediate: Green Synthesis and Applications toward the Removal of Pollutants, *ACS Appl. Polym. Mater.*, 2021, **3**(2), 789–800.

30 C. Feng, G. Xu, W. Xie, S. Zhang, C. Yao and Y. Xu, Polytriazine porous networks for effective iodine capture, *Polym. Chem.*, 2020, **11**(16), 2786–2790.

31 H. Li, X. Ding and B. H. Han, Porous Azo-Bridged Porphyrin–Phthalocyanine Network with High Iodine Capture Capability, *Chem.–Eur. J.*, 2016, **22**(33), 11863–11868.

32 S. Yao, W.-H. Fang, Y. Sun, S.-T. Wang and J. Zhang, Mesoporous assembly of aluminum molecular rings for iodine capture, *J. Am. Chem. Soc.*, 2021, **143**(5), 2325–2330.

33 P. Chen, X. He, M. Pang, X. Dong, S. Zhao and W. Zhang, Iodine capture using Zr-based metal–organic frameworks (Zr-MOFs): adsorption performance and mechanism, *ACS Appl. Mater. Interfaces*, 2020, **12**(18), 20429–20439.

34 Y. Xu, H. Yu, B. Shi, S. Gao, L. Zhang, X. Li, X. Liao and K. Huang, Room-temperature synthesis of hollow carbazole-based covalent triazine polymers with multiactive sites for efficient iodine capture-catalysis cascade application, *ACS Appl. Polym. Mater.*, 2020, **2**(8), 3704–3713.

35 C. Falaise, C. Volkringer, J. Facqueur, T. Bousquet, L. Gasnot and T. Loiseau, Capture of iodine in highly stable metal–organic frameworks: a systematic study, *Chem. Commun.*, 2013, **49**(87), 10320–10322.

36 Z.-Q. Jiang, F. Wang and J. Zhang, Adsorption of iodine based on a tetrazolate Framework with microporous cages and mesoporous cages, *Inorg. Chem.*, 2016, **55**(24), 13035–13038.

37 D. F. Sava, M. A. Rodriguez, K. W. Chapman, P. J. Chupas, J. A. Greathouse, P. S. Crozier and T. M. Nenoff, Capture of volatile iodine, a gaseous fission product, by zeolitic imidazolate framework-8, *J. Am. Chem. Soc.*, 2011, **133**(32), 12398–12401.

38 M. Huang, L. Yang, X. Li and G. Chang, An indole-derived porous organic polymer for the efficient visual colorimetric capture of iodine in aqueous media via the synergistic effects of cation–π and electrostatic forces, *Chem. Commun.*, 2020, **56**(9), 1401–1404.

39 D. An, L. Li, Z. Zhang, A. M. Asiri, K. A. Alamry and X. Zhang, Amino-bridged covalent organic polycalix [4] arenes for ultra efficient adsorption of iodine in water, *Mater. Chem. Phys.*, 2020, **239**, 122328.

40 A. Sen, S. Sharma, S. Dutta, M. M. Shirolkar, G. K. Dam, S. Let and S. K. Ghosh, Functionalized Ionic Porous Organic Polymers Exhibiting High Iodine Uptake from Both the Vapor and Aqueous Medium, *ACS Appl. Mater. Interfaces*, 2021, **13**(29), 34188–34196.

41 K. Kabiri, H. Omidian and M. Zohuriaan-Mehr, Novel approach to highly porous superabsorbent hydrogels:

synergistic effect of porogens on porosity and swelling rate, *Polym. Int.*, 2003, **52**(7), 1158–1164.

42 M. Saed Hussein, T. Pei Leng, A. Razak Rahmat, F. Zainuddin, Y. Cheow Keat, K. Suppiah and Z. Salem Alsagayar, The effect of sodium bicarbonate as blowing agent on the mechanical properties of epoxy, *Mater. Today: Proc.*, 2019, **16**, 1622–1629.

43 A. Shakeri, S. M. M. Babaheydari, H. Salehi and S. R. Razavi, Reduction of the Structure Parameter of Forward Osmosis Membranes by Using Sodium Bicarbonate as Pore-Forming Agent, *Langmuir*, 2021, **37**(24), 7591–7599.

44 B. H. Min and K. Y. Jung, Improved porosity and ionic sorption capacity of carbon particles prepared by spray pyrolysis from an aqueous sucrose/NaHCO3/TEOS solution, *RSC Adv.*, 2017, **7**(34), 21314–21322.

45 M. Hartman, K. Svoboda, M. Pohořelý and M. Šyc, Thermal Decomposition of Sodium Hydrogen Carbonate and Textural Features of Its Calcines, *Ind. Eng. Chem. Res.*, 2013, **52**(31), 10619–10626.

46 F. Ambroz, T. J. Macdonald, V. Martis and I. P. Parkin, Evaluation of the BET Theory for the Characterization of Meso and Microporous MOFs, *Small Methods*, 2018, **2**(11), 1800173.

47 T. Madrakian, A. Afkhami, M. A. Zolfigol, M. Ahmadi and N. Koukabi, Application of modified silica coated magnetite nanoparticles for removal of iodine from water samples, *Nano-Micro Lett.*, 2012, **4**(1), 57–63.

48 S. Sharma, S. Let, A. V. Desai, S. Dutta, G. Karuppasamy, M. M. Shirolkar, R. Babarao and S. K. Ghosh, Rapid, selective capture of toxic oxo-anions of Se (iv), Se (vi) and As (v) from water by an ionic metal–organic framework (iMOF), *J. Mater. Chem. A*, 2021, **9**(10), 6499–6507.

49 M. J. Manos and M. G. Kanatzidis, Metal sulfide ion exchangers: superior sorbents for the capture of toxic and nuclear waste-related metal ions, *Chem. Sci.*, 2016, **7**(8), 4804–4824.

50 S. Salai Cheettu Ammal, S. Ananthavel, P. Venuvanalingam and M. Hegde, UVPES and ab Initio Molecular Orbital Studies on the Electron Donor−Acceptor Complexes of Bromine with Methylamines, *J. Phys. Chem. A*, 1997, **101**(6), 1155–1159.

51 Y. Liao, J. Weber, B. M. Mills, Z. Ren and C. F. Faul, Highly efficient and reversible iodine capture in hexaphenylbenzene-based conjugated microporous polymers, *Macromolecules*, 2016, **49**(17), 6322–6333.

52 M. Xu, T. Wang, L. Zhou and D. Hua, Fluorescent conjugated mesoporous polymers with N, N-diethylpropylamine for the efficient capture and real-time detection of volatile iodine, *J. Mater. Chem. A*, 2020, **8**(4), 1966–1974.

53 S. Wang, Y. Liu, Y. Ye, X. Meng, J. Du, X. Song and Z. Liang, Ultrahigh volatile iodine capture by conjugated microporous polymer based on N, N, N′, N′-tetraphenyl-1, 4-phenylenediamine, *Polym. Chem.*, 2019, **10**(20), 2608–2615.

54 J. Chang, H. Li, J. Zhao, X. Guan, C. Li, G. Yu, V. Valtchev, Y. Yan, S. Qiu and Q. Fang, Tetrathiafulvalene-based covalent organic frameworks for ultrahigh iodine capture, *Chem. Sci.*, 2021, **12**(24), 8452–8457.

55 Y. Xie, T. Pan, Q. Lei, C. Chen, X. Dong, Y. Yuan, J. Shen, Y. Cai, C. Zhou, I. Pinnau and Y. Han, Ionic Functionalization of Multivariate Covalent Organic Frameworks to Achieve an Exceptionally High Iodine-Capture Capacity, *Angew. Chem., Int. Ed.*, 2021, **60**(41), 22432–22440.

